remote sensing

MDPI

Article

Performance of Solar-Induced Chlorophyll Fluorescence in Estimating Water-Use Efficiency in a Temperate Forest

Xiaoliang Lu [1,2], Zhunqiao Liu [2,3], Yuyu Zhou [4], Yaling Liu [5] and Jianwu Tang [2,*]

1 Department of Forest Ecosystems and Society, Oregon State University, Corvallis, OR 97331, USA; luxiaoliangresearch@gmail.com
2 The Ecosystems Center, Marine Biological Laboratory, Woods Hole, MA 02543, USA; liuzhunqiao@gmail.com
3 School of life sciences, Nanjing University, Xianlin Campus,163 Xianlin Road, Nanjing, Jiangsu 210023, China
4 Department of Geological and Atmospheric Sciences, Iowa State University, Ames, IA 50011, USA; yuyuzhou@iastate.edu
5 Department of Earth and Environmental Engineering, Columbia University, 500 W. 120th St, 918 S. W. Mudd Hall, 500, New York, NY 10027, USA; yl3937@columbia.edu
* Corresponding: jtang@mbl.edu; Tel.: +1-508-289-7162

Received: 28 March 2018; Accepted: 6 May 2018; Published: 20 May 2018

Abstract: Water-use efficiency (WUE) is a critical variable describing the interrelationship between carbon uptake and water loss in land ecosystems. Different WUE formulations (WUEs) including intrinsic water use efficiency (WUE_i), inherent water use efficiency (IWUE), and underlying water use efficiency (uWUE) have been proposed. Based on continuous measurements of carbon and water fluxes and solar-induced chlorophyll fluorescence (SIF) at a temperate forest, we analyze the correlations between SIF emission and the different WUEs at the canopy level by using linear regression (LR) and Gaussian processes regression (GPR) models. Overall, we find that SIF emission has a good potential to estimate IWUE and uWUE, especially when a combination of different SIF bands and a GPR model is used. At an hourly time step, canopy-level SIF emission can explain as high as 65% and 61% of the variances in IWUE and uWUE. Specifically, we find that (1) a daily time step by averaging hourly values during daytime can enhance the SIF-IWUE correlations, (2) the SIF-IWUE correlations decrease when photosynthetically active radiation and air temperature exceed their optimal biological thresholds, (3) a low Leaf Area Index (LAI) has a negative effect on the SIF-IWUE correlations due to large evaporation fluxes, (4) a high LAI in summer also reduces the SIF-IWUE correlations most likely due to increasing scattering and (re)absorption of the SIF signal, and (5) the observation time during the day has a strong impact on the SIF-IWUE correlations and SIF measurements in the early morning have the lowest power to estimate IWUE due to the large evaporation of dew. This study provides a new way to evaluate the stomatal regulation of plant-gas exchange without complex parameterizations.

Keywords: solar-induced chlorophyll fluorescence; water use efficiency; leaf area index; observation time; regression analysis

1. Introduction

Ecosystem water use efficiency (WUE), typically defined as the ratio between gross primary productivity (GPP) and evapotranspiration (ET), is typically used to indicate tradeoff between carbon uptake and water losses in land ecosystems. Many studies have shown that changes in WUE are related to variations in a variety of environmental factors including aerosol loading [1], land use change [2,3],

climate change [4], and nitrogen deposition [5]. When transpiration (T) dominates ET, variations in WUE reflect how plants regulate carbon-water exchange processes through stomata. However, WUE also varies with vapor pressure deficit (VPD) [6,7], which complicates correlations between WUE and plant conditions. Recently, more physiologically meaningful formulations have been proposed to quantify the interrelationship between carbon and water cycles. Intrinsic WUE (WUE_i), which is defined as the ratio between GPP and surface conductance (Gs), was introduced [8,9]. Gs that is used to represent water loss from ecosystems is usually estimated by inverting the Penman–Monteith equation [10,11] (hereinafter referred to as P-M equation). Studies have shown that WUE_i is more appropriate to describe the capacity of different plants to regulate how much water is lost per unit carbon acquired [12,13], because Gs implicitly considers the impacts of related environmental factors. However, it is hard to estimate WUE_i, especially at a large spatial scale, because a large number of difficultly measured variables are needed to calculate Gs. Furthermore, Gs also contains the effects of canopy architecture, which is not related to stomatal closure. After some simplifying assumptions, Beer et al. [14] proposed a much more simplified formulation called inherent water use efficiency (IWUE) as a proxy for the WUE_i. IWUE, which is defined as the product of VPD and WUE, significantly removes obscurities induced by variations in VPD. IWUE is more reflective of carbon and water exchanges via stomata [14] than WUE, and it has been wildly used to quantify the responses of plants to environmental controls including drought stress [15], nitrogen deposition [16], and rising CO_2 concentration [17]. Note that IWUE was developed by assuming the ratio of inner leaf over ambient partial pressure of CO_2 (C_i/C_a) to be constant. However, studies have shown that VPD may change C_i/C_a [6,18]. To account for the effect of VPD on C_i/C_a, Katul et al. [19] proposed underlying water use efficiency (uWUE), which is defined as $uWUE = GPP*VPD^{0.5}/ET$ and they showed that uWUE is more related to plant physiological regulation of carbon uptake and water losses at the sub-daily time scale [20].

Although IWUE and uWUE are relatively simple and have a potential to describe mechanisms controlling carbon and water exchanges through stomata, their estimation at large spatial scales is still challenging. At regional or global scales, both GPP and ET are estimated from either processed-based or semi-empirical models, which use remotely sensed and/or meteorological variables as inputs [21,22]. However, their performances may suffer from uncertainties in assumptions, inputs, and parameters. For example, it is common that estimated ET has an error greater than 50% [22–24]. Satellite-based estimates typically capture less than 60% of the variance in WUE even at sites with accurate measurements [25]. Thus, efforts on pursing other efficient ways in estimating large scale WUE are highly needed.

More recently, studies have shown that solar-induced chlorophyll fluorescence (SIF) emission has a close correlation with carbon assimilation [26–29]. Plants convert captured incoming solar radiation into three different pathways: assimilating carbon from the atmosphere into organic compounds (i.e., photosynthesis), heat dissipation (i.e., non-photochemical quenching (NPQ), and SIF emission. SIF emission is in the range of 640–850 nm and has two peaks: one in the red spectral region (640–700 nm) and the other in the near infrared region (700–850 nm). Recent satellite-based studies [30,31] showed that SIF emission has good performance in assessing the impacts of water stress on photosynthetic activities. The field-based study [32] also confirmed that SIF emission estimated T with better accuracy than processed-based approaches such as the P-M and the Priestley-Taylor equation [33]. Considering good performance of SIF in predicting both GPP and T, one would expect SIF may have a potential to estimate WUE, WUE_i, IWUE, and uWUE (hereinafter referred to as WUEs) when ET is mainly determined by T.

By using continuous measurements of SIF emission, carbon exchange, and latent heat in a temperate deciduous forest, we aim to evaluate the ability of SIF emission in tracking WUEs under different environmental conditions. We implemented this study in the following aspects: (1) analyzing correlations between SIF emission and WUEs at the hourly and daily time steps by using the linear and nonlinear regression analysis, (2) exploring whether multi-bands SIF have more powerful capacity to

estimate WUEs, and (3) investigating how SIF-WUEs correlations respond to variations in the different environmental conditions including VPD, solar radiation, air temperature, leaf area index (LAI), and observation time.

2. Materials and Methods

2.1. Site Description

The experiment site is located in the Harvard Forest, Petersham, Massachusetts, USA (42°32′07.2″N 72°11′23.4″W). The forest has a mean canopy height of 22 m and a mean stand age of about 80 years. The dominant forest types are American beech (*Fagus grandifolia* Ehrh.), red oak (*Quercus rubra)*, and red maple (*Acer rubrum* L.). The forests have four distinct seasons: leaves initiate in spring, maintain green in summer, change color in autumn, and fall off in the winter. The climate is characterized by a cool and moist temperate. The mean daily air temperature (T_{air}) was 6.8 °C in 2014 when this study was implemented. The precipitation (*Prcp*) in 2014 was 1283 mm, which was higher than the mean average of 1050 mm during 1950–2015. Accordingly, VPD remained at a relatively low level. The mean daily daytime VPD was 0.66 kPa in 2014; VPD had higher values in the period from June to August, showing an increase in demand for water in summer.

2.2. Instrumentations and Datasets

Canopy-level SIF is measured by using a spectrometer (HR2000+, OceanOptics, Inc., Dunedin, FL, USA) mounted 5 m above the forest top. This spectrometer has a spectral resolution of 0.13 nm over the range from 679.6–775.6 nm and it had a field of view (FOV) of 5 m on top of the canopy. The spectrometer is linked with two fiber optics with a shutter (FOS-2x2-TTL, OceanOptics, Inc.). One fiber collects downwelling incident solar irradiance (I) and the other collects canopy upwelling radiance (L). I and L were measured every 5 min during the growing season (May–September). Note that upwelling radiance contains contributions from both reflected solar energy and SIF emission. The previous studies [26,34] showed that these two components can be described by some simple mathematical functions at absorption lines. In this study, we used the three absorption lines including O_2-B at 687 nm, water vapor at 720 nm, and O_2-A at 761 nm. Reflectance and SIF emission at these three lines are expressed by the second order Taylor polynomials. Theoretically, it requires at least six measurements of L and I to retrieve a single instantaneous SIF emission. Please see Supplementary Materials for the details. Instantaneous SIF measurements in the selected bands are then aggregated to hourly values. SIF emission at the three absorption lines are referred to as SIF_{687}, SIF_{720}, and SIF_{761}, respectively.

Turbulent fluxes of latent heat (λE) were measured using the eddy covariance (EC) method [35] at the Environmental Measurement Station (EMS) site, which is close (about 1.4 km) to the SIF measurements site. The original λE was converted into hourly ET (kg H_2O/m^2/hour). Hourly GPP (g C/m^2/hour) was obtained from the EMS tower in 2014 via the Harvard Forest Long-Term Ecological Research program. LAI was collected by using a LAI-2000 Plant Canopy Analyzer (LI-COR, Lincoln, NE, USA). We measured LAI daily during spring season (May and June) and autumn senescence (September and October) periods in 2014, and monthly in the mature period (July–August). Other meteorological variables, including VPD (kPa), rain fall (*Prcp*, mm/hour), friction velocity (*UST*, m/s), net radiation (Rn, W/m^2), air temperature (T_{air}, Celsius degree °C), wind speed (U, m/s), and air pressure (P, kPa), were also measured at an hourly time step. Because forest at the site has a dense canopy, we assume ET is dominated by transpiration during the growing season [36]. To reduce the influence of evaporation from the intercepted rainfall, we excluded data when precipitation exceeded 1 mm/hour and 72 h after these events. We also removed measurements with sun zenith angle larger than 60 degree [37]. From hourly ET, GPP, and VPD data, we calculated ecosystem-level hourly WUE, IWUE, and uWUE. To estimate hourly WUE_i, Gs was calculated by inverting the P-M equation. Daily daytime SIF emission, WUE, WUE_i, IWUE, uWUE, and other related meteorological variables were aggregated into daily values by averaging half-hourly or hourly values measured between 7:00 a.m.

and 5:00 p.m. local time. The daily values were excluded from the analysis if more than 4 hourly values were missed in one day. We used the moving average approach to remove outliers in the related time series. Specifically, values that deviated from the mean of a 5-point moving window by more than 25% were excluded and missing values were replaced by an inverse distance weighting method using adjacent "clean" points in time series.

2.3. Regression Models

We use two types of regression models to calculate correlations between SIF emission and WUE_S. One is the linear regression (LR) model and the other is the adaptive, nonlinear regression called the Gaussian process regression (GPR) model [38]. The regression analyses were implemented on the hourly and daily time series. The coefficient of determination (R^2) was used to quantify the strength of SIF emission in predicting WUEs. For all analysis, statistically significant differences were set at $p < 0.05$. All the statistical and regression analyses are made using Matlab Statistics Toolbox 2016b (The Math Works, Inc., Natick, MA, USA).

In addition to these single SIF bands retrieved at the three absorption lines (SIF_{687}, SIF_{720} and SIF_{761}), both recent model-based [39] and field-based studies [32,40] showed that combinations of SIF bands tend to enhance SIF-GPP/T correlations. Therefore, we added the following two SIF band combinations to the analysis: (1) SIF emission at the O_2-B and O_2-A absorption lines (hereinafter referred to as SIF_{687} and SIF_{761}), and (2) SIF emission at the three main absorption lines including O_2-B, water vapor, and O_2-A (hereinafter SIF_{687}, SIF_{720}, and SIF_{761}).

3. Results

3.1. Temporal Patterns of WUEs and SIF Emission

The mean of summer (June to August, three months) daytime WUE, WUE_i, IWUE, and uWUE were 0.14 g C/kg H_2O, 13.45 umol C/mmol H_2O, 0.14 g C hPa/kg H_2O and 0.13 g C hPa/kg H_2O, respectively (Figure 1), which were much higher than their values in the spring/winter seasons. It suggested that plants became more efficient in using water resources when they were water stressed. Among the four formulations, IWUE and uWUE demonstrated a stronger seasonal pattern, as both of them showed a rapid increase in late April and May, maintained a high value for about two months in summer, and started to decline in September (Figure 1c,d). Compared to IWUE, uWUE showed a relatively smaller range and variability in summer (Figure 1d), most likely due to the use of the square root of VPD. In contrast, WUE and WUE_i showed less substantial changes in the spring and autumn seasons and had a longer plateau of high values (Figure 1a,b). Note that WUE_i contained more missing values, reflecting additional difficulties in estimating WUE_i (Figure 1b).

The three SIF time series also demonstrated a clear seasonal pattern. Among the three SIF bands, SIF_{687} showed less variation in both spring and autumn seasons (Figure 2a) and remained roughly stable, with values around 0.14 $mW/m^2/sr/nm$ from the late spring to early autumn. In contrast, the dynamics of SIF_{720} and SIF_{761} in 2014 showed a stronger seasonal pattern, as they increased very fast in spring, maintained stability in the mature period, and dropped rapidly in autumn (Figure 2b,c). Among these three SIF bands, SIF_{761} had the most pronounced emission, as its hourly emission peak reached about 1.6 $mW/m^2/sr/nm$, which was about 5 times higher than the emission peak of SIF_{687} (Figure 2a,c). The number of SIF_{687} observations is less than that of SIF_{761}, which indicates that strong a (re)absorption effect and weak emitted energy in red SIF may cause additional difficulties in retrieving SIF_{687}.

Remote Sens. **2018**, *10*, x FOR PEER REVIEW 5 of 19

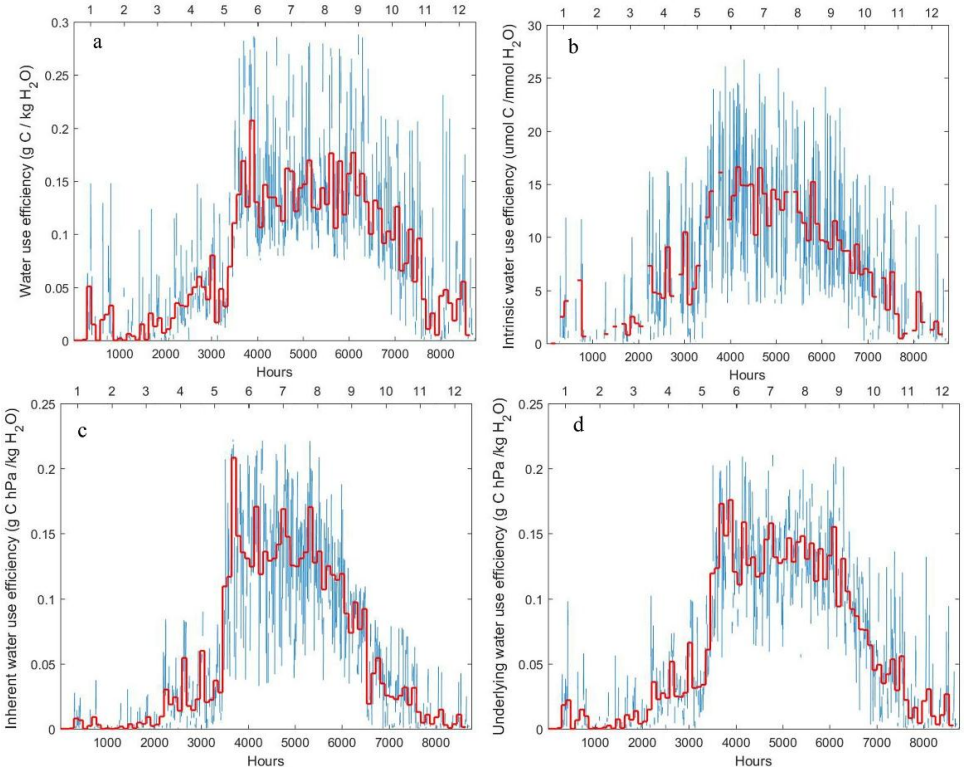

Figure 1. The time series of hourly (**a**) water use efficiency (WUE, g C/kg H_2O); (**b**) intrinsic water use efficiency (WUE_i, umol C /mmol H_2O); (**c**) inherent water use efficiency (IWUE, g C hPa /kg H_2O) and (**d**) underlying water use efficiency (uWUE, g C hPa /kg H_2O) at the Harvard Forest site in 2014. The red lines represent 4-day daytime averages. The values in the top *x*-axes represent months.

Figure 1. The time series of hourly (**a**) water use efficiency (WUE, g C/kg H_2O); (**b**) intrinsic water use efficiency (WUE_i, umol C /mmol H_2O); (**c**) inherent water use efficiency (IWUE, g C hPa /kg H_2O) and (**d**) underlying water use efficiency (uWUE, g C hPa /kg H_2O) at the Harvard Forest site in 2014. The red lines represent 4-day daytime averages. The values in the top *x*-axes represent months.

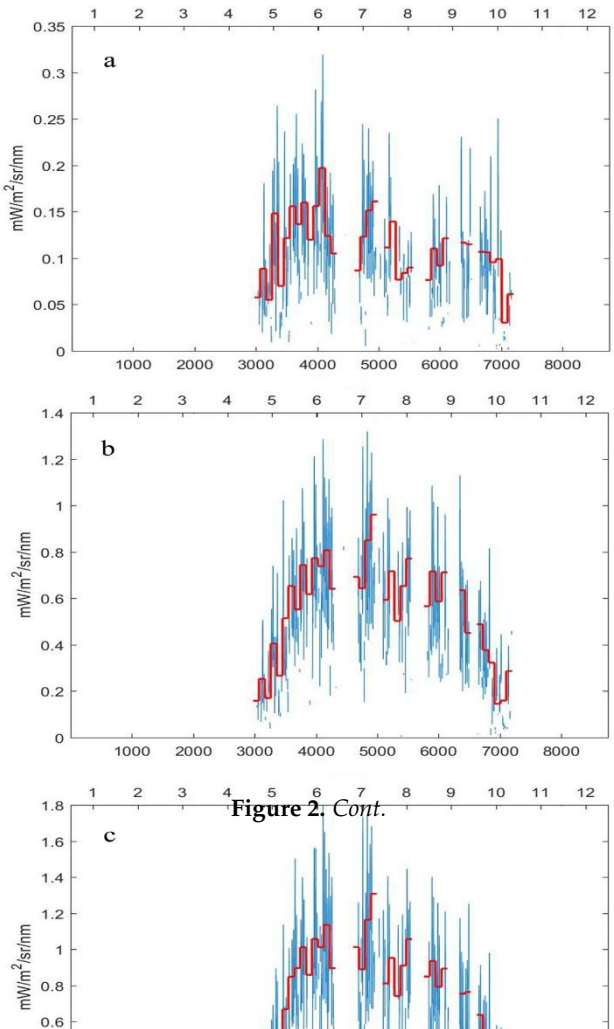

Figure 2. *Cont.*

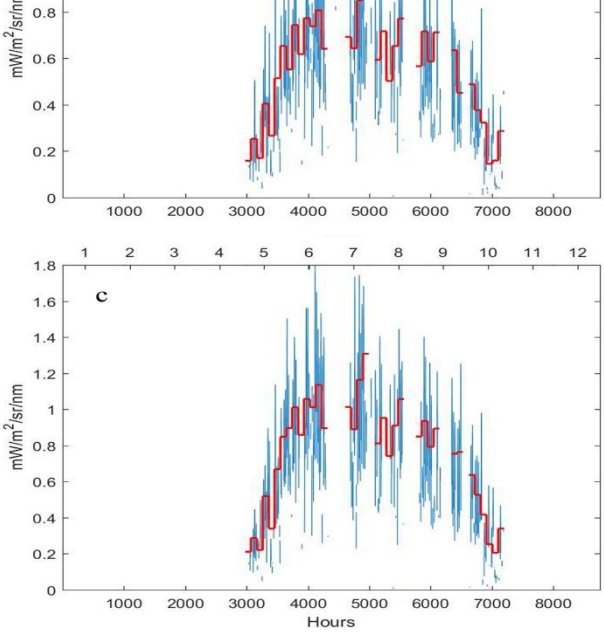

Figure 2. The time series of hourly (**a**) SIF_{687} (mW/m²/sr/nm), (**b**) SIF_{720} (mW/m²/sr/nm) and (**c**) SIF_{761} (mW/m²/sr/nm) at the Harvard Forest site in 2014. The red lines represent 4-day daytime averages. The values in the top *x*-axes represent months.

3.2. Overall Performance of SIF Emission in Predicting Hourly and Daily WUEs

3.2.1. Performance in Predicting Hourly WUEs

The coefficients of determination (R^2) show that SIF_{687} is a weak predictor of the selected WUEs. It shows almost no correlation with all the four WUEs, and its best R^2 is only 0.17 when it is used to estimate IWUE (Table 1). In comparison to SIF_{687}, SIF_{720} obtains an obvious improvement in predicting IWUE and uWUE and it accounts for 48% and 36% variances, respectively, by using the GPR models (Table 1). However, SIF_{720} has weak correlations with WUE and WUE_i, as they can only explain at most 8% and 14% of the variance in them (Table 1). Among the three single SIF bands, SIF_{761} shows the greatest strength in predicting hourly IWUE and uWUE and it determines 52% and 34% of the variability in them, but SIF_{761} again shows poor correlations with WUE and WUE_i even when the GPR models are used (Table 1).

Our results confirm that the SIF band combinations provide better predictive power than the single SIF bands when they are used individually. Both of the two combinations have the best performance in estimating IWUE. The LR results show that the combination of SIF_{687} and SIF_{761} account for 49% variability in hourly IWUE (Table 1). The more SIF bands are used in the combination, the greater the likelihood of yielding a stronger predictive power. The combination of SIF_{687}, SIF_{720}, and SIF_{761} produces further improvement, which governs about 50% variability in IWUE (Table 1). Both of the two R^2 values are better than that provided by SIF_{761}, which is the best single SIF band. Also, the GPR models further enhance the predictive power of the band combinations. When the GPR models are used, the two combinations can determine 62% and 65% of the IWUE variances, respectively (Table 1).

Table 1. The correlation coefficient (R^2) between the SIF bands and water use efficiency (WUE), intrinsic water use efficiency (WUE_i), inherent water use efficiency (iWUE), and underlying water use efficiency (uWUE), by using linear regression analysis (LR) and Gaussian process regression (GPR), respectively. All datasets have an hourly time step and are from between 7 a.m. and 5 p.m. local time.

SIF bands	WUE		WUE_i		IWUE		uWUE	
	LR	GPR	LR	GPR	LR	GPR	LR	GPR
SIF_{687}	0.09	0.14	0.07	0.12	0.13	0.17	0.02	0.05
SIF_{720}	0.00	0.08	0.11	0.14	0.42	0.48	0.23	0.36
SIF_{761}	0.00	0.08	0.14	0.17	0.44	0.52	0.25	0.34
SIF_{687}, SIF_{761}	0.24	0.44	0.15	0.20	0.49	0.62	0.39	0.55
SIF_{687}, SIF_{720}, SIF_{761}	0.23	0.46	0.15	0.28	0.59	0.65	0.36	0.61

In fact, the band combinations also produce considerable improvements in R^2 with the other three WUEs over using the single SIF bands (Table 1). For example, the combination of SIF_{687}, SIF_{720}, and SIF_{761} achieves R^2 of 0.46, 0.28, and 0.61, with WUE, WUE_i, and uWUE, respectively, whereas single SIF_{761} yields R^2 of 0.08, 0.17 and 0.34 for these three WUEs (Table 1).

3.2.2. Performance in Predicting Daily WUEs

Longer time steps, such as daily, are more suitable in many applications. A recent model-based study [41] showed that SIF-GPP correlations were enhanced at both leaf and canopy scales when longer time steps were considered. Therefore, we also calculated SIF-WUEs' correlations at a daily time scale by using the LR and GPR models. Because the number of valid daily observations is much smaller, we used a cross-validation to test for possible overfit in the regressions. Specifically, all daily measurements (55) were randomly split into two groups: (a) a training group containing 60% of all daily measurements, used to develop the regression models, and (b) a testing group containing the other 40% that were used to test the performance of the predictions. We did not find an obvious difference in the R^2 from the two groups (see the Supplementary Materials), which confirms no overfitting in building the regression models. The below results, describing the relationships between SIF and WUEs at a daily time step, were derived from all the daily measurements.

Overall, our results show that all the SIF-WUEs' correlations are enhanced after aggregating from hourly to daily scale (Table 2). SIF_{687} is still the weakest predictor for all the four WUEs, and its best R^2, 0.41, is achieved when it is used to predict daily IWUE (Table 2). It shows this negative effect due to the (re)absorption in red SIF emission, which is still strong at a daily time step. In contrast, SIF_{720} and SIF_{761} exhibit much higher correlations with the WUEs after the temporal aggregation, especially when the GPR models are used (Table 2). Again, SIF_{761} produces the strongest correlations with the WUEs among the three single SIF bands, as it captures 62% and 65% variance in daily IWUE for the LR and GPR, respectively (Table 2). SIF_{761} can also explain 44%, 47%, and 57% of the variance in daily WUE, WUE_i, and uWUE, respectively (Table 2). Although SIF_{720} is not as strong a predictor as SIF_{761}, it is still superior to SIF_{687}. For example, SIF_{720} accounts for 53% and 62% of the variability in daily IWUE by using the LR and GPR models, respectively (Table 2).

Table 2. The correlation coefficient (R^2) between the SIF bands and daily water use efficiency (WUE), intrinsic water use efficiency (WUE_i), inherent water use efficiency (IWUE), and underlying water use efficiency (uWUE) by using linear regression analysis (LR) and Gaussian processes regression (GPR), respectively. The daily values were aggregated from hourly measurements between 7 a.m. and 5 p.m. local time.

SIF bands	WUE		WUE_i		IWUE		uWUE	
	LR	GPR	LR	GPR	LR	GPR	LR	GPR
SIF_{687}	0.00	0.00	0.08	0.00	0.21	0.41	0.11	0.37
SIF_{720}	0.17	0.38	0.30	0.34	0.53	0.62	0.43	0.47
SIF_{761}	0.17	0.44	0.37	0.47	0.62	0.65	0.49	0.57
SIF_{687}, SIF_{761}	0.19	0.51	0.51	0.53	0.64	0.65	0.52	0.60
SIF_{687}, SIF_{720}, SIF_{761}	0.24	0.58	0.52	0.65	0.67	0.70	0.58	0.63

At a daily time step, the band combinations demonstrate further improvements in their correlations with the WUEs. The combination of SIF_{687} and SIF_{761} can explain more than 50% variance in all WUEs when the GPR models were used (Table 2), and can also explain more than 60% of the variance in IWUE and uWUE, respectively (Table 2). The combination using all the three single SIF bands provided modest improvements, as it can explain 70% and 63% of the variance in daily IWUE and uWUE with the GPR models (Table 2). Also, the combination of SIF_{687}, SIF_{720}, and SIF_{761} is a fairly good predictor of daily WUE and WUE_i, which provides R^2 of 0.58 and 0.65, respectively (Table 2).

3.3. Responses of the SIF-IWUE Relationship to the Environmental Factors

Both model-based and field-based studies [39–41] have shown that SIF-GPP correlations may deteriorate when solar radiation, VPD, and air temperature exceed their optimal biological thresholds. Furthermore, the recent study [32] indicated that the performance of SIF emission in predicting T was also dependent on a variety of environmental, biogeophysical, and biogeochemical factors. Therefore, it is critical to investigate how SIF-WUEs relationship changes under different environmental conditions. Because SIF emission produces the strongest correlations with IWUE (Tables 1 and 2), we analyze how the SIF-IWUE relationships respond to changes in the different environmental factors including VPD, solar radiation, air temperature, LAI, and observation time.

3.3.1. Effects of VPD on Correlations between IWUE and SIF Emission

VPD is typically used to represent water stress on plants [21]. Strong water stress may weaken the link between photosynthesis activities and SIF emission [30,31]. Further, one important motivation to develop the different WUE formulations is to remove the nonlinear effect of VPD on T. Thus, it is essential to assess whether the SIF-IWUE relationship is still affected by VPD. To do so, we calculated the R^2 between SIF emission and IWUE at an hourly time step under three VPD levels: (1) low: VPD $\leq$ 0.5 kPa, (2) medium: 0.5 kPa < VPD $\leq$ 1.0 kPa, and (3) high: VPD > 1.0 kPa.

The results from the LR models indicate that VPD has no clear negative impact on the SIF-IWUE correlations (Figure 3a). For example, SIF_{761} has almost the same performance by explaining 25%, 17%, and 25% of the variance in IWUE under these three VPD levels, respectively (Figure 3a). Further, VPD also has no obvious influence on the performance of the SIF band combinations. The combination of SIF_{687}, SIF_{720}, and SIF_{761} determines 44% and 41% of the variance in IWUE under the low and intermediate VPD levels and its performance only decreases slightly to 39% under high VPD values (Figure 3a). Again, the results from the GPR models show that the SIF-IWUE correlations have a relatively low sensitivity to VPD (Figure 3b). For instance, SIF_{761} determines 39% of variability in IWUE when VPD values are high, and the counterparts decrease to 37% and 22% when VPD values are low and medium (Figure 3b). The predictive power of combined SIF bands for IWUE shows a moderate improvement under the high VPD level. The R^2 of the combination of SIF_{687}, SIF_{687}, and SIF_{761} shows a correlation of R^2 = 0.69 against IWUE for the high VPD level, while it decreases to 0.62 and 0.53 under the low and intermediate VPD levels, respectively (Figure 3b).

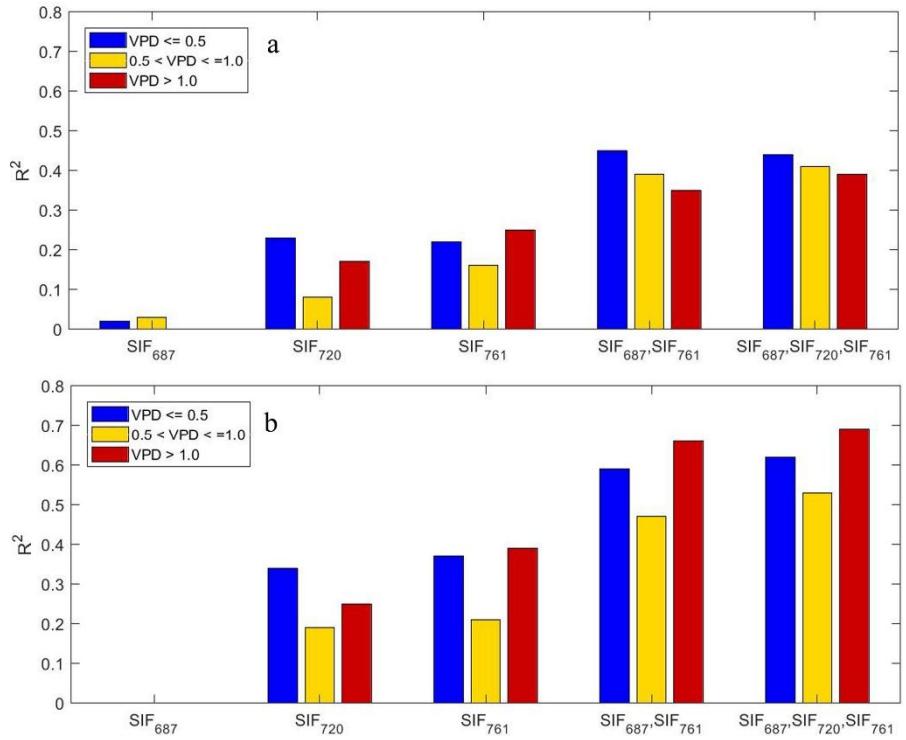

Figure 3. The effect of vapor pressure deficit (VPD, kPa) on the coefficients of determination (R^2) between inherent water use efficiency (IWUE) and the selected single SIF bands and their combinations by using (**a**) linear regression analysis and (**b**) Gaussian processes regression, respectively. The blue, yellow, and red bars represent R^2 for data with VPD ≤ 0.5 kPa, 0.5 kPa < VPD ≤ 1.0 kPa, and VPD > 1.0 kPa, respectively. All data have an hourly time resolution and belong to the period between 7 a.m. and 5 p.m. local time.

Figure 3. The effect of vapor pressure deficit (VPD, kPa) on the coefficients of determination (R^2) between inherent water use efficiency (IWUE) and the selected single SIF bands and their combinations by using (**a**) linear regression analysis and (**b**) Gaussian processes regression, respectively. The blue, yellow, and red bars represent R^2 for data with VPD ≤ 0.5 kPa, 0.5 kPa < VPD ≤ 1.0 kPa, and VPD > 1.0 kPa, respectively. All data have an hourly time resolution and belong to the period between 7 a.m. and 5 p.m. local time.

3.3.2. Effects of Solar Radiation on IWUE-SIF Correlations

3.3.2. Effects of Solar Radiation on IWUE-SIF Correlations

The intensity of SIF emission depends on incoming solar radiation. However, excessive light may cause plants to invoke various protection mechanisms to release excessive energy as NPQ [42], which tends to weaken SIF-GPP correlations [40]. Also, too strong solar radiation may also result in lower R^2 between SIF and T [32]. So, it is necessary to investigate how changes in radiation regime affect the SIF-IWUE relationship. Based on the relationship of PAR-GPP (Figure S1), we used 1300 μmol photons/m²/s as the threshold to separate all hourly data into two groups: (1) PAR saturation group and (2) no PAR saturation group.

The intensity of SIF emission depends on incoming solar radiation. However, excessive light may cause plants to invoke various protection mechanisms to release excessive energy as NPQ [42], which tends to weaken SIF-GPP correlations [40]. Also, too strong solar radiation may also result in lower R^2 between SIF and T [32]. So, it is necessary to investigate how changes in radiation regime affect the SIF-IWUE relationship. Based on the relationship of PAR-GPP (Figure S1), we used 1300 μmol photons/m²/s as the threshold to separate all hourly data into two groups: (1) PAR saturation group and (2) no PAR saturation group.

Our results show that the PAR saturation has a negative effect on the SIF-IWUE correlations but with limited impacts. The highest R^2 provided by SIF_{761} is 0.50 under no PAR saturation, whereas it only has a small decrease to 0.41 under the PAR saturation (Figure 4). Further, the SIF band combinations seem to provide a strong resistance to radiation stress. Under the no saturation condition, the combination of SIF_{687}, SIF_{720}, and SIF_{761} can explain 54% and 66% variance in IWUE for the LR and GPR models, respectively (Figure 4). When PAR reaches saturation, its performance only has a minimal decline with 48% and 63%, respectively (Figure 4).

Our results show that the PAR saturation has a negative effect on the SIF-IWUE correlations but with limited impacts. The highest R^2 provided by SIF_{761} is 0.50 under no PAR saturation, whereas it only has a small decrease to 0.41 under the PAR saturation (Figure 4). Further, the SIF band combinations seem to provide a strong resistance to radiation stress. Under the no saturation condition, the combination of SIF_{687}, SIF_{720}, and SIF_{761} can explain 54% and 66% variance in IWUE for the LR and GPR models, respectively (Figure 4). When PAR reaches saturation, its performance only has a minimal decline with 48% and 63%, respectively (Figure 4).

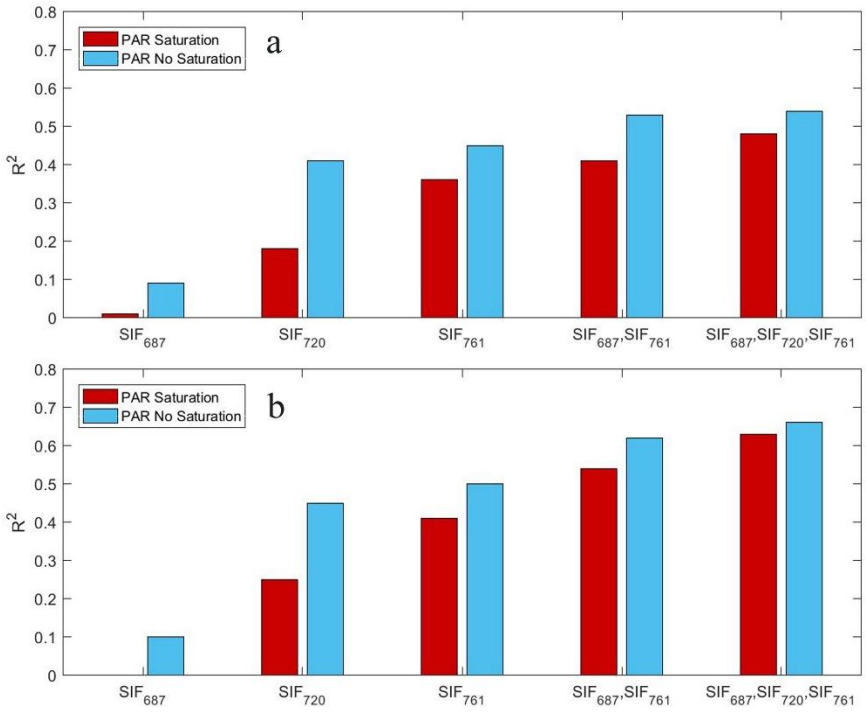

Figure 4. The effect of intensity of Photosynthetically Active Radiation (PAR) on the coefficients of determination (R^2) between inherent water use efficiency (IWUE) and the selected single SIF bands and their combinations by using (**a**) linear regression analysis and (**b**) Gaussian processes regression, respectively. The blue/red bars represent R^2 from data with PAR less/more than 1300 μmol photons/m^2/s. All data have an hourly time resolution and belong to the period between 7 a.m. and 5 p.m. local time.

Figure 4. The effect of intensity of Photosynthetically Active Radiation (PAR) on the coefficients of determination (R^2) between inherent water use efficiency (IWUE) and the selected single SIF bands and their combinations by using (**a**) linear regression analysis and (**b**) Gaussian processes regression, respectively. The blue/red bars represent R^2 from data with PAR less/more than 1300 μmol photons/m^2/s. All data have an hourly time resolution and belong to the period between 7 a.m. and 5 p.m. local time.

Considering the fact that remotely-sensed datasets typically use cloud fractions to select high-quality data, we calculate the clearness index (K) [43] at the site level (Figure S2) and only use data with $K > 0.8$ to analyze the SIF-IWUE correlations (Table 3). Our results show that all the SIF-IWUE correlations only have moderate decreases. Under the clear sky condition, for example, SIF_{761} has a small decrease in its R^2 with IWUE of 0.05 and 0.06 for LR and GPR, respectively (Table 3). Again, the band combinations produce a more stable performance, especially when the nonlinear GPR models are used. Combining SIF emission at the three absorption lines can still determine 46% and 60% of variance in hourly IWUE (Table 3).

Considering the fact that remotely-sensed datasets typically use cloud fractions to select high-quality data, we calculate the clearness index (K) [43] at the site level (Figure S2) and only use data with $K > 0.8$ to analyze the SIF-IWUE correlations (Table 3). Our results show that all the SIF-IWUE correlations only have moderate decreases. Under the clear sky condition, for example, SIF_{761} has a small decrease in its R^2 with IWUE of 0.05 and 0.06 for LR and GPR, respectively (Table 3). Again, the band combinations produce a more stable performance, especially when the nonlinear GPR models are used. Combining SIF emission at the three absorption lines can still determine 46% and 60% of variance in hourly IWUE (Table 3).

Table 3. The correlation coefficient (R^2) between the SIF bands and inherent water use efficiency (IWUE) by using the linear regression analysis (LR) and Gaussian processes regression (GPR), respectively. All the datasets had an hourly time step and were measured between 7 a.m. and 5 p.m. local time with clearness index (K) higher than 0.8. The numbers in the parentheses are the R^2 calculated from all the hourly data acquired between 7 a.m. and 5 p.m. local time.

SIF bands		LR	GPR
SIF_{687}		0.04 (0.17)	0.04 (0.17)
SIF_{720}		0.27 (0.48)	0.30 (0.48)
SIF_{761}		0.39 (0.44)	0.46 (0.52)
SIF_{687}, SIF_{761}		0.43 (0.49)	0.54 (0.62)
SIF_{687}, SIF_{720}, SIF_{761}		0.46 (0.59)	0.60 (0.65)

SIF bands		LR	GPR
SIF_{687}		0.04 (0.17)	0.04 (0.17)
SIF_{720}		0.27 (0.48)	0.30 (0.48)
SIF_{761}		0.39 (0.44)	0.46 (0.52)
SIF_{687}, SIF_{761}		0.43 (0.49)	0.54 (0.62)
SIF_{687}, SIF_{720}, SIF_{761}		0.46 (0.59)	0.60 (0.65)

3.3.3. Effects of Air Temperature on IWUE-SIF Correlations

Too high air temperature reduces the activation of RuBISCO and thus photosynthesis rates. Under heat stress, plants tend to release more absorbed energy by NPQ, which may weaken SIF emission and photosynthesis activities [32]. Also, water loss through transpiration may increase to

3.3.3. Effects of Air Temperature on IWUE-SIF Correlations

Too high air temperature reduces the activation of RuBISCO and thus photosynthesis rates. Under heat stress, plants tend to release more absorbed energy by NPQ, which may weaken SIF emission and photosynthesis activities [32]. Also, water loss through transpiration may increase to maintain the energy balance in plants when the water supply is not limiting [40]. Both of the two mechanisms may deteriorate the relationship between SIF emission and IWUE. To analyze the influences of T_{air} on the SIF-IWUE relationship, we calculated the R^2 between SIF emission and IWUE for three T_{air} groups. Hourly T_{air} between 7 am and 5 pm. local time were separated into three groups: (1) low: $T_{air} \leq 14$ °C, (2) medium: 14 °C < T_{air} < 22 °C, and (3) high: $T_{air} \geq 22$ °C.

Remote Sens. **2018**, *10*, x FOR PEER REVIEW 11 of 19
maintain the energy balance in plants when the water supply is not limiting [40]. Both of the two mechanisms may deteriorate the relationship between SIF emission and IWUE. To analyze the influences of T_{air} on the SIF-IWUE relationship, we calculated the R^2 between SIF emission and IWUE for three T_{air} groups. Hourly T_{air} between 7 am and 5 pm. local time were separated into three groups: (1) low: $T_{air} \leq 14$ °C, (2) medium: 14 °C < T_{air} < 22 °C, and (3) high: $T_{air} \geq 22$ °C.

When LR models are used, the predictive power of SIF is negatively related to T_{air}. For example, SIF_{761} can explain about 40% of the variance in IWUE in the low T_{air} group, but its performance decreases to 27% for high T_{air} (Figure 5a). The combination of SIF_{687}, SIF_{720}, and SIF_{761} also benefits from low T_{air} with an R^2 of 0.48 and 0.32 for the low and high T_{air}, respectively (Figure 5a). However, we find that the SIF-IWUE correlation tends to increase with an increasing T_{air} when GPR models are used (Figure 5b). For instance, SIF_{761} show R^2 = 0.41 and 0.47 in the low and high T_{air}, respectively (Figure 5b). Further, the SIF-IWUE correlations demonstrate more increases with T_{air} when the band combinations are used, as the combination of SIF_{687}, SIF_{720}, and SIF_{761} has R^2 = 0.55, 0.62 and 0.57 with increasing in T_{air} (Figure 5b). The different responses of IWUE to T_{air} yielded by LR and GPR show that SIF-IWUE relationships become more nonlinear with increasing T_{air}.

When LR models are used, the predictive power of SIF is negatively related to T_{air}. For example, SIF_{761} can explain about 40% of the variance in IWUE in the low T_{air} group, but its performance decreases to 27% for high T_{air} (Figure 5a). The combination of SIF_{687}, SIF_{720}, and SIF_{761} also benefits from low T_{air} with an R^2 of 0.48 and 0.32 for the low and high T_{air}, respectively (Figure 5a). However, we find that the SIF-IWUE correlation tends to increase with an increasing T_{air} when GPR models are used (Figure 5b). For instance, SIF_{761} show R^2 = 0.41 and 0.47 in the low and high T_{air}, respectively (Figure 5b). Further, the SIF-IWUE correlations demonstrate more increases with T_{air} when the band combinations are used, as the combination of SIF_{687}, SIF_{720}, and SIF_{761} has R^2 = 0.55, 0.62 and 0.57 with increasing in T_{air} (Figure 5b). The different responses of IWUE to T_{air} yielded by LR and GPR show that SIF-IWUE relationships become more nonlinear with increasing T_{air}.

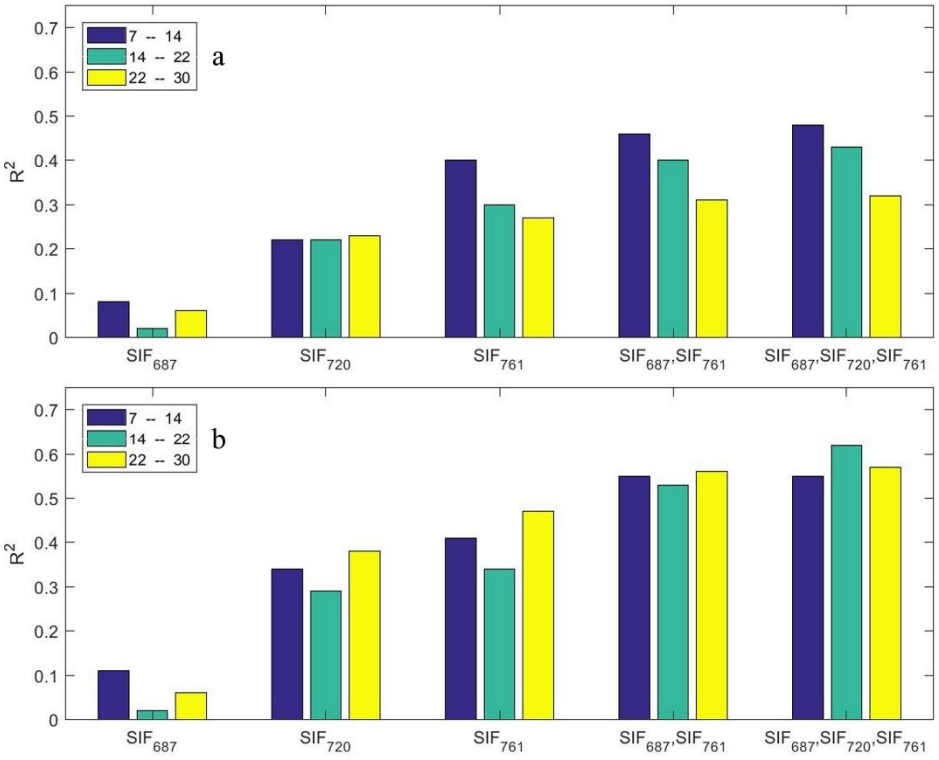

Figure 5. The effect of air temperature (T_{air}, °C) on the coefficients of determination (R^2) between IWUE and the selected single SIF bands and their combinations by using (**a**) linear regression analysis and (**b**) Gaussian processes regression, respectively. The blue, green and yellow bars represent R^2 from data with $T_{air} \leq 14$ °C, 14 °C < T_{air} < 22 °C, and $T_{air} \geq 22$ °C, respectively. All data have an hourly time resolution and belong to the period between 7 a.m. and 5 p.m. local time.

3.3.4. Effects of LAI on IWUE-SIF Correlations

An increase in LAI may result in more loss of SIF emission due to reabsorption and scattering processes [29], which may deteriorate relationships between SIF and WUEs. Our previous studies have shown that a dense canopy tends to negatively affect SIF-GPP/T relationships at a canopy level [32,40]. Therefore, it is important to evaluate how different LAI values affect linkage between SIF signals and IWUE. For this purpose, we calculated the SIF-IWUE correlations from hourly data under three different LAI groups: (1) low: 0 < LAI ≤ 2.0, (2) medium: 2.0 < LAI ≤ 4.5, and (3) high: LAI > 4.5.

Remote Sens. 2018, 10, x FOR PEER REVIEW 12 of 19

3.3.4. Effects of LAI on IWUE-SIF Correlations

An increase in LAI may result in more loss of SIF emission due to reabsorption and scattering processes [29], which may deteriorate relationships between SIF and WUEs. Our previous studies have shown that a dense canopy tends to negatively affect SIF-GPP/*T* relationships at a canopy level [32,40]. Therefore, it is important to evaluate how different LAI values affect linkage between SIF signals and IWUE. For this purpose, we calculated the SIF-IWUE correlations from hourly data under three different LAI groups: (1) low: $0 < LAI \leq 2.0$, (2) medium: $2.0 < LAI \leq 4.5$, and (3) high: $LAI \geq 4.5$.

The SIF-IWUE correlations decline when LAI values are in the low and high groups (Figure 6). In the low LAI group, all the selected single SIF bands explain less than 35% of variance in IWUE for the GPR models. The SIF band combinations provide marginal improvements, and the combination of SIF_{687}, SIF_{720}, and SIF_{761} shows the correlations with IWUE with R^2 of 0.29 and 0.45 for the LR and GPR when LAI is lower than 2.0 (Figure 6). When the LAI is the highest ($LAI > 4.5$), the SIF-IWUE correlations are considerably weakened, as all the single SIF bands show $R^2 < 0.04$ and the use of GPR only provided very limited improvements (Figure 6). Although the combinations of SIF bands generally provide a better performance in estimating IWUE, the combination of SIF_{687}, SIF_{720}, and SIF_{761}, the best predictor, only shows R^2 of 0.06 and 0.04 for LR and GPR, respectively (Figure 6).

The SIF-IWUE correlations are highest when LAI values are in the medium group (Figure 6). For example, the R^2 between SIF_{761} and IWUE was 0.37 and 0.41 in the group for the LR and GPR model, which are higher than those when LAI are in the low and high groups (Table 1). The SIF band combinations obtain further improvements, particularly, the combination of SIF_{687}, SIF_{720}, and SIF_{761} shows the best correlations with IWUE with R^2 of 0.49 and 0.58 for the LR and GPR, respectively (Figure 6a,b).

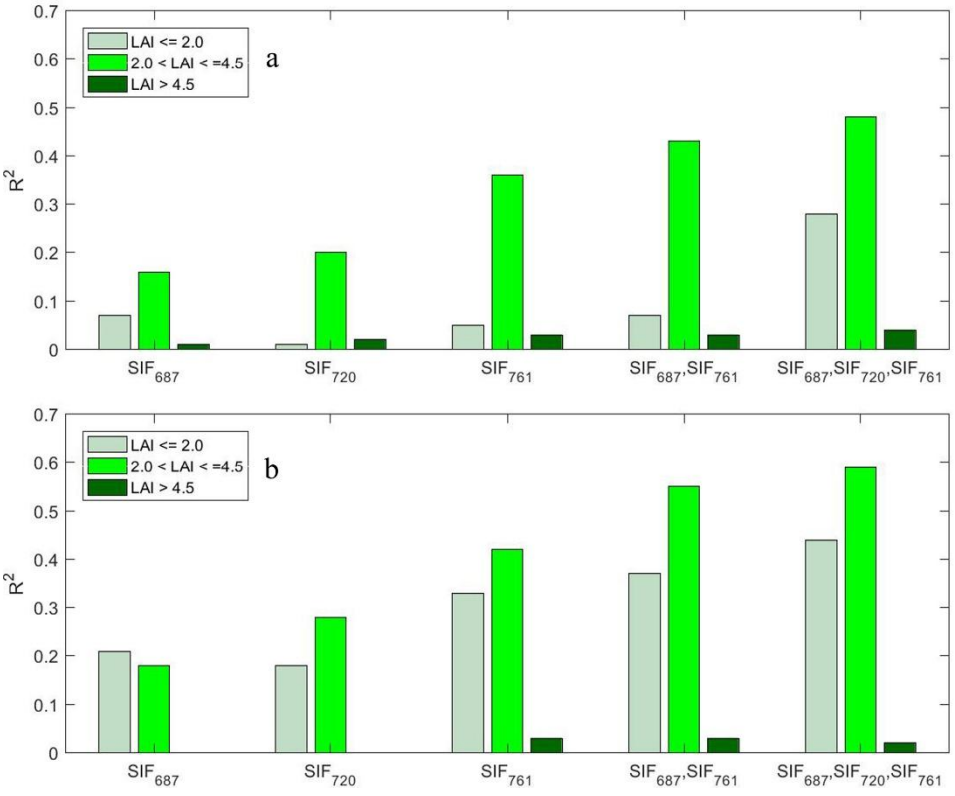

Figure 6. The effect of leaf area index (LAI) on the coefficients of determination (R^2) between inherent water use efficiency (IWUE) and the selected single SIF bands and their combinations by using (**a**) linear regression analysis and (**b**) Gaussian processes regression, respectively. The LAI ranges are included in the legends. All data have an hourly time resolution and belong to the period between 7 a.m. and 5 p.m. local time.

3.3.5. Effects of Observation Time on IWUE-SIF Correlations

The SIF-IWUE correlations are highest when LAI values are in the medium group (Figure 6). For example, the R^2 between SIF_{761} and IWUE was 0.37 and 0.41 in the group for the LR and GPR model, which are higher than those when LAI are in the low and high groups (Table 1). The SIF band combinations obtain further improvements, particularly, the combination of SIF_{687}, SIF_{720}, and SIF_{761} shows the best correlations with IWUE with R^2 of 0.49 and 0.58 for the LR and GPR, respectively (Figure 6a,b).

SIF emission has successfully been retrieved from measurements provided by space-borne spectrometer, such as GOSAT [44], GOME-2 [45], SCanning Imaging Absorption SpectroMeter for Atmospheric CHartographY (SCIAMACHY) [46], and Orbiting Carbon Observatory-2 (OCO-2) [47]. They have the following different overpass times: 09:30 a.m. for GOME-2, 10:00 for SCIAMACHY, 12:00 for GOAST, and 13:30 for OCO-2. Also, both WUEs and SIF emission have strong diurnal cycles (Figures 1 and 2). For an appropriate use of remotely-sensed SIF data for retrieving WUEs at a large scale, it is particularly important to assess the impact of observation time of day on the SIF-IWUE

shows the best correlations with IWUE with R^2 of 0.49 and 0.58 for the LR and GPR, respectively (Figure 6a,b).

3.3.5. Effects of Observation Time on IWUE-SIF Correlations

SIF emission has successfully been retrieved from measurements provided by spaceborne spectrometer such as GOSAT [44], GOME-2 [45], SCanning Imaging Absorption SpectroMeter for Atmospheric CHartographY (SCIAMACHY) [46], and Orbiting Carbon Observatory 2 (OCO-2) [47]. They have the following different overpass times: 09:30 a.m. for GOME-2, 10:00 for SCIAMACHY, 12:00 for GOAST, and 13:30 for OCO-2. Also, both WUEs and SIF emission have strong diurnal cycles (Figures 1 and 2). For an appropriate use of remotely-sensed SIF data for retrieving WUEs at a large scale, it is particularly important to assess the impact of observation time of day on the SIF-IWUE relationship. To do so, we separate hourly SIF emission and IWUE into three different groups: morning (7–10), midday (10–15), and afternoon (15–17).

The results suggest that the observation time exerts a clear impact on the SIF-IWUE relationship at the canopy level. In comparison to R^2 in the morning and midday, there are systematically stronger correlations in the afternoon (Figure 7). Also, the SIF-IWUE correlations at midday are better than those in the morning (Figure 7). In fact, the SIF-IWUE correlations in the afternoon are better than those derived from the daily daytime dataset (Tables 2 and 3). For example, SIF_{761} has a strong correlation with IWUE in the afternoon, with R^2 reaching a value of 0.60 and 0.69 for the LR and GPR (Figure 7). However, its performance is as high as 0.52 and 0.39 in the morning and midday, respectively (Figure 7). In the afternoon, the band combinations, together with the GPR, also yield a predictive advantage over those derived over the whole daytime (Table 3, Figure 7b). The combination of SIF_{687}, SIF_{720}, and SIF_{761} has the strongest correlation with IWUE with R^2 achieving 0.79 for GPR (Figure 7b), while its performance decreases to 0.71 and 0.46 when it is used to predict IWUE in the morning and midday with using the GPR models (Figure 7b).

Remote Sens. **2018**, *10*, x FOR PEER REVIEW 13 of 19

relationship. To do so, we separate hourly SIF emission and IWUE into three different groups: morning (7–10), midday (10–15), and afternoon (15–17).

The results suggest that the observation time exerts a clear impact on the SIF-IWUE relationship at the canopy level. In comparison to R^2 in the morning and midday, there are systematically stronger correlations in the afternoon (Figure 7). Also, the SIF-IWUE correlations at midday are better than those in the morning (Figure 7). In fact, the SIF-IWUE correlations in the afternoon are better than those derived from the daily daytime dataset (Tables 2 and 3). For example, SIF_{761} has a strong correlation with IWUE in the afternoon, with R^2 reaching a value of 0.60 and 0.69 for the LR and GPR (Figure 7). However, its performance is as high as 0.52 and 0.39 in the morning and midday, respectively (Figure 7). In the afternoon, the band combinations, together with the GPR, also yield a predictive advantage over those derived over the whole daytime (Table 3, Figure 7b). The combination of SIF_{687}, SIF_{720}, and SIF_{761} has the strongest correlation with IWUE with R^2 achieving 0.79 for GPR (Figure 7b), while its performance decreases to 0.71 and 0.46 when it is used to predict IWUE in the morning and midday with using the GPR models (Figure 7b).

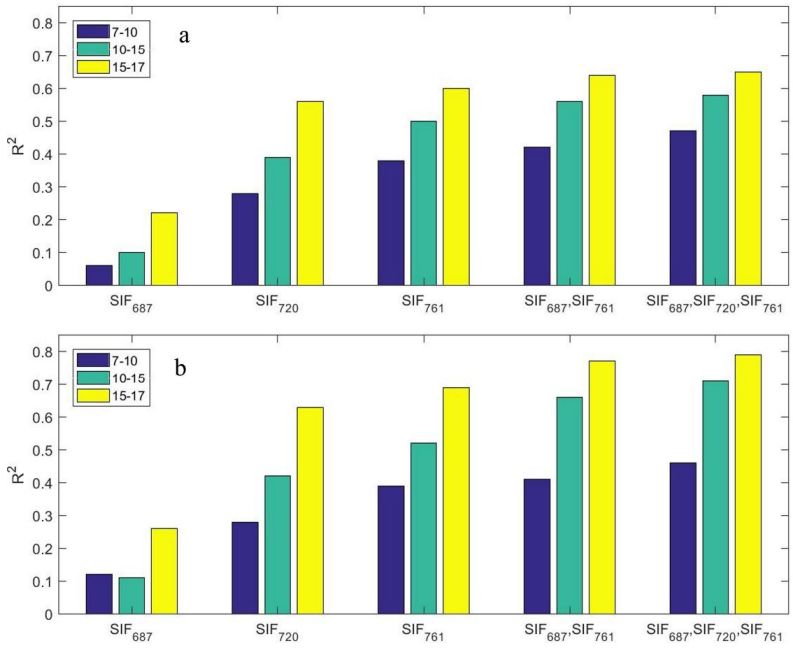

Figure 7. The effect of diurnal observation time on the coefficients of determination (R^2) between inherent water use efficiency (IWUE) and the selected single SIF bands and their combinations by using (**a**) linear regression analysis and (**b**) Gaussian processes regression, respectively. All data have an hourly time resolution. The blue, green, and yellow bars represent R^2 for data with observation time at 7–10 a.m., 10 a.m.–15 p.m., and 15–17 p.m., respectively.

Figure 7. The effect of diurnal observation time on the coefficients of determination (R^2) between inherent water use efficiency (IWUE) and the selected single SIF bands and their combinations by using (**a**) linear regression analysis and (**b**) Gaussian processes regression, respectively. All data have an hourly time resolution. The blue, green, and yellow bars represent R^2 for data with observation time at 7–10 a.m., 10 a.m.–15 p.m., and 15–17 p.m., respectively.

4. Discussion

Overall, we find that SIF emission has the potential to predict the carbon-water exchange process through stomata. Among the four different WUE formulations, SIF emission shows a good performance in estimating IWUE and uWUE. The likely explanation is that the consideration of VPD in IWUE and uWUE largely remove the nonlinear effect of VPD on T. In contrast, SIF emission shows weaker correlations with WUE and WUE_i, especially at an hourly time step. Because variations in the traditional WUE (ET/GPP) still contain impacts of VPD, which cannot be tracked by SIF, the correlations between WUE and SIF are typically low. Although WUE_i is derived from the physical-

4. Discussion

Overall, we find that SIF emission has the potential to predict the carbon-water exchange process through stomata. Among the four different WUE formulations, SIF emission shows a good performance in estimating IWUE and uWUE. The likely explanation is that the consideration of VPD in IWUE and uWUE largely remove the nonlinear effect of VPD on *T*. In contrast, SIF emission shows weaker correlations with WUE and WUE_i, especially at an hourly time step. Because variations in the traditional WUE (ET/GPP) still contain impacts of VPD, which cannot be tracked by SIF, the correlations between WUE and SIF are typically low. Although WUE_i is derived from the physical-based model, it involves numerous not-easily measured environmental variables, which makes it difficult to use at a large scale. Also, the simplification assumptions needed in inverting the P-M equation likely bring strong noises in its time series, which tends to undermine the performance of SIF emission in predicting WUE_i. When the daily daytime data are used, SIF emission demonstrates a more powerful predictive capability of all these four WUEs. The recent studies [32,41] have shown that SIF emission has a better performance in estimating both GPP and *T* at a longer time step. More field- and model-based works are needed to analyze the reason for stronger SIF-IWUE correlations under a longer temporal resolution.

Combining different SIF bands provides stronger correlations with IWUE than those when single SIF bands were used individually. SIF emission at different spectra contains information on the physiological status of plants. For example, most of red SIF emission comes from the photosystem II (PSII) [48]. SIF emission in the near-infrared region contains contributions from both PSI and PSII [49] and it was found to be closely correlated with GPP at both global [50,51] and local scales [52]. Thus, SIF band combination should contain more complete information on plant physiological conditions. In this study, we only used the combination of SIF emission at the three absorption lines. Full exploitation of the complete SIF spectrum may provide further better performance of SIF emission in predicting WUEs [32,39]. It is important to note that the performance of the full SIF spectrum depends on: (1) the accuracy of the sensor, and (2) the approach used to reconstruct full SIF emission. Our spectrometer is not the newest. Furthermore, the SCOPE model [39], which is currently used to build full SIF, may not be the best option. More efforts are highly needed in better extracting the potential of full SIF. The combinations of different SIF bands may bring more nonlinear behaviors. Also, our results show that IWUE-SIF correlations show more non-linear behaviors when plants are under stressful conditions. In both cases, nonlinear regression models such as GPR should be used.

We find that a variety of physiological and environmental factors affect SIF-IWUE relationships. The interactions of these factors further complicate the link between SIF emission and IWUE. Among them, VPD is found to have less of an effect on the SIF-IWUE correlations (Figure 3). The stable SIF-IWUE correlations under different VPD values show that (1) incorporation of VPD into IWUE largely removes impacts of VPD on GPP and *T*, and (2) VPD in 2014 showed no clear negative effect on SIF-GPP and SIF-*T* correlations. However, it is important to note that the precipitation at the study site in 2014 was higher than the multi-year average precipitation. The relatively wet condition in 2014 did not allow us to fully analyze variations in SIF-IWUE relationships under severe water stress. SIF-IWUE correlations may further deteriorate when more severe drought conditions occur. Thus, more field experiments are needed to evaluate SIF-IWUE relationships under stronger water stress.

Our results show too high or too low LAI values that tend to deteriorate SIF-IWUE correlations. Under low LAI values, more evaporation from bare soil should enhance nontranspiration flux, which may weaken SIF-IWUE correlations. High LAI values have both positive and negative effects on SIF-IWUE correlations. On the one hand, canopy closure reduces solar radiation received by the ground and thus results in less contribution from soil evaporation, which tends to enhance SIF-IWUE correlations. On the other hand, a dense canopy at high LAIs leads to more (re)absorption in red SIF and stronger scattering in near infrared SIF, both of which decouple the link between SIF emission and latent energy measured at top of the canopy. Our results show that the negative effect associated with high LAIs is more pronounced when LAI is higher than 4.5. It suggests that a canopy radiation

transfer model [53] may be needed to account for SIF losses due to scattering/absorption processes, especially when SIF is used to estimate IWUE in ecosystems with dense canopy.

Previous studies have shown that observation time in the day has a limited impact on both SIF-GPP and SIF-*T* correlations [32,40,41]. However, SIF-IWUE correlations vary as a function of the observation time during the day and they are strongest in the afternoon. This phenomenon can be explained by variations in evaporation of dew present in the canopy and soil. Specifically, the SIF-IWUE correlation is considerably weakened in the morning, particularly in the early morning [54], when evaporation of dew, a nontranspiration flux, contributes a large fraction of latent flux measured at the top of canopy. Our results suggest that SIF-IWUE correlations derived from remotely sensed SIF data, with an early morning overpass time such as GOME-2, may contain large uncertainties. A model [55], which predicts occurrence and duration of dew events may be needed. When the simulated dew is high, SIF emission may be not suitable for predicting IWUE.

The response of the SIF-IWUE correlations to air temperature shows they are affected by confounding factors. Theoretically, both SIF-GPP and SIF-*T* correlations [32,41] degrade under heat stress due to more energy release through heat dissipation. Although higher air temperature in the afternoon may cause lower SIF-GPP and SIF-*T* correlations, we find that the benefit, due to less dew evaporation in the afternoon, may largely counteract these negative effects. However, it is important to note that the study site had no strong heat stress in 2014 such that further experiments are needed to evaluate SIF-IWUE correlations in high air temperature. Furthermore, relatively cool air temperature in the morning may enhance both SIF-GPP and SIF-*T* correlations [32,41], while more evaporation of dew tends to weaken the capability of SIF to predict *T*.

Our results show that the intensity of PAR has a limited negative effect on SIF-IWUE correlations. Nonlinear models such as GPR should be used when solar radiation is close to the saturation. Also, the band combinations, especially the one using SIF_{687}, SIF_{720}, and SIF_{761}, provide stable performance under the PAR saturation. We also find that a clear sky condition, which may be used to select good-quality satellite observations, has a marginal impact on SIF-IWUE correlations. It confirms that remotely sensed SIF datasets can be used to derive SIF-IWUE correlations. Data with k>0.8 are more likely measured under the PAR saturation condition. Our results show that the intensity of PAR has a limited negative effect on the SIF-IWUE correlations such that these correlations tend to have a limited decrease under different sky clearness conditions.

The authors are aware of several limitations in this study. Compared to new spectrometers such as QE Pro spectrometer (OceanOptics, Inc, Dunedin, Florida), the signal-to-noise ratio (250:1) of our spectrometer is relatively lower such that measurements of SIF emission may contain more noise, especially in the red SIF emission. More important, recent studies [56,57] have shown that near-infrared radiation such as SIF_{761} also contains information on canopy structure such that a directional effect may lead to uncertainties in retrieving SIF signals. Also, SIF signals measured in this study are only part of total SIF emission, while measurements of GPP and *T* contain contributions from the whole canopy. SIF-IWUE relationships derived from total canopy SIF emission should be more robust, especially under high LAI values. To reduce these uncertainties, a process-based radiation transfer model can be used to separate physiologically and directionally induced changes in SIF emission [58,59]. Finally, it is important to note that one important assumption in developing SIF-WUEs models is that transpiration flux dominates ET. Therefore, SIF-IWUE correlations would be weaker in wetlands or irrigated lands where nontranspiration flux may be significant.

5. Conclusions

By using continuous records of SIF measurements, carbon and latent heat fluxes, this study shows that SIF emission can serve as a good predictor of IWUE and uWUE, two WUE formulations with consideration of VPD effect, in a temperate deciduous forest. However, SIF emission has weaker correlations with WUE and WUE_i. The predictive capability of SIF emission is dependent on a variety of environmental, biogeophysical, and biogeochemical factors including solar radiation, LAI,

observation time, and air temperature. In particular, we find that (1) the models using SIF band combinations provide more a powerful capacity to estimate IWUE than the models using single SIF bands, (2) a temporal aggregation to the daily scale can further enhance the SIF-IWUE correlations, especially when SIF band combination and non-linear models are considered, (3) PAR saturation shows a limited negative effect on the SIF-IWUE correlations, but more experiments are highly needed, (4) too high LAIs largely reduce the SIF-IWUE correlations due to (re)absorption and scattering of SIF emission, (5) large nontranspiration flux due to soil and dew evaporation significantly reduces the SIF-IWUE correlations, and (6) it is desirable to use SIF emission measured in the afternoon for retrieving IWUE when dew evaporation is low.

This study provides a new SIF application in understanding the nexus between carbon uptake and transpiration loss in terrestrial ecosystems. In comparison to physical models that are inputs demanding and complex, a SIF-based approach offers a simple but powerful way to investigate carbon uptake and water loss in plants at a large spatial scale.

Supplementary Materials: The following are available online at http://www.mdpi.com/2072-4292/10/5/796/s1. **Figure S1**: The responses of hourly daytime (a) gross primary production (GPP, umol CO_2 m/s) and (b) transpiration (T, mm/hour) to incident photosynthetically active radiation (PAR, umol photons/m^2/s) during the growing season in 2014. **Figure S2**: The hourly clearness index at the Harvard site in 2014. **Table S1**: The correlation coefficient (R^2) of the training and testing groups in predicting and daily WUEs by using the linear regression analysis (LR) and Gaussian processes regression (GPR), respectively. This section also describes the details in estimating SIF emission from irradiance and radiance measurements.

Author Contributions: X.L. and Z.L. conceived and designed the study, and interpreted the results; X.L. carried out the analyses and wrote the paper; Y.L., Y.Z. and J.T. contributed to the manuscript revision. Z.L. and J.T. made important contributions to the field experiments.

Acknowledgments: We would like to thank Harvard Forest for providing site and logistic support during our research. The water flux data were downloaded from the Harvard Forest data archive (PI: J. William Munger). This research was supported by U.S. Department of Energy Office of Biological and Environmental Research Grant DE-SC0006951, National Science Foundation Grants DBI 959333 and AGS-1005663, and the University of Chicago and the MBL Lillie Research Innovation Award to Jianwu Tang. This study was also supported by the open project grant (LBKF201701) of Key Laboratory of Land Surface Pattern and Simulation, Chinese Academy of Sciences.

Conflicts of Interest: The authors declare no conflict of interest.

References

1. Lu, X.L.; Chen, M.; Liu, Y.L.; Miralles, D.G.; Wang, F.M. Enhanced water use efficiency in global terrestrial ecosystems under increasing aerosol loadings. *Agric. For. Meteorol.* **2017**, *237*, 39–49. [CrossRef]
2. Kaplan, J.O.; Krumhardt, K.M.; Zimmermann, N.E. The effects of land use and climate change on the carbon cycle of Europe over the past 500 years. *Glob. Chang. Biol.* **2012**, *18*, 902–914. [CrossRef]
3. Sterling, S.M.; Ducharne, A.; Polcher, J. The impact of global land-cover change on the terrestrial water cycle. *Nat. Clim. Chang.* **2013**, *3*, 385–390. [CrossRef]
4. Niu, S.L.; Xing, X.R.; Zhang, Z.; Xia, J.Y.; Zhou, X.H.; Song, B.; Li, L.H.; Wan, S.Q. Water-use efficiency in response to climate change: From leaf to ecosystem in a temperate steppe. *Glob. Chang. Biol.* **2011**, *17*, 1073–1082. [CrossRef]
5. Huang, M.T.; Piao, S.L.; Sun, Y.; Ciais, P.; Cheng, L.; Mao, J.F.; Poulter, B.; Shi, X.Y.; Zeng, Z.Z.; Wang, Y.P. Change in terrestrial ecosystem water-use efficiency over the last three decades. *Glob. Chang. Biol.* **2015**, *21*, 2366–2378. [CrossRef] [PubMed]
6. Tang, J.W.; Bolstad, P.V.; Ewers, B.E.; Desai, A.R.; Davis, K.J.; Carey, E.V. Sap flux-upscaled canopy transpiration, stomatal conductance, and water use efficiency in an old growth forest in the great lakes region of the united states. *J. Geophys. Res. Biogeosci.* **2006**, *111*, 12. [CrossRef]
7. Linderson, M.L.; Mikkelsen, T.N.; Ibrom, A.; Lindroth, A.; Ro-Poulsen, H.; Pilegaard, K. Up-scaling of water use efficiency from leaf to canopy as based on leaf gas exchange relationships and the modeled in-canopy light distribution. *Agric. For. Meteorol.* **2012**, *152*, 201–211. [CrossRef]

8. Nock, C.A.; Baker, P.J.; Wanek, W.; Leis, A.; Grabner, M.; Bunyavejchewin, S.; Hietz, P. Long-term increases in intrinsic water-use efficiency do not lead to increased stem growth in a tropical monsoon forest in western Thailand. *Glob. Chang. Biol.* **2011**, *17*, 1049–1063. [CrossRef]
9. Liu, X.H.; Wang, W.Z.; Xu, G.B.; Zeng, X.M.; Wu, G.J.; Zhang, X.W.; Qin, D.H. Tree growth and intrinsic water-use efficiency of inland riparian forests in northwestern China: Evaluation via δ13C and δ18O analysis of tree rings. *Tree Physiol.* **2014**, *34*, 966–980. [CrossRef] [PubMed]
10. Penman, H.L. Natural evaporation from open water, bare soil and grass. *Proc. R. Soc. Lond. Ser. A* **1948**, *193*, 120–145. [CrossRef]
11. Monteith, J.L. Evaporation and environment. In *The State and Movement of Water in Living Organisms. Symposium of the Society of Experimental Biology*; Fogg, G.E., Ed.; Society of Experimental Biology, Cambridge University Press: Swansea, UK, 1965; Volume 19, pp. 205–234.
12. Condon, A.G.; Richards, R.A.; Rebetzke, G.J.; Farquhar, G.D. Improving intrinsic water-use efficiency and crop yield. *Crop Sci.* **2002**, *42*, 122–131. [CrossRef] [PubMed]
13. Tomeo, N.J.; Rosenthal, D.M. Variable mesophyll conductance among soybean cultivars sets a tradeoff between photosynthesis and water-use-efficiency open. *Plant Physiol.* **2017**, *174*, 241–257. [CrossRef] [PubMed]
14. Beer, C.; Ciais, P.; Reichstein, M.; Baldocchi, D.; Law, B.E.; Papale, D.; Soussana, J.F.; Ammann, C.; Buchmann, N.; Frank, D.; et al. Temporal and among-site variability of inherent water use efficiency at the ecosystem level. *Glob. Biogeochem. Cycles* **2009**, *23*, GB2018. [CrossRef]
15. Grossiord, C.; Gessler, A.; Granier, A.; Pollastrini, M.; Bussotti, F.; Bonal, D. Interspecific competition influences the response of oak transpiration to increasing drought stress in a mixed Mediterranean forest. *For. Ecol. Manag.* **2014**, *318*, 54–61. [CrossRef]
16. Leonardi, S.; Gentilesca, T.; Guerrieri, R.; Ripullone, F.; Magnani, F.; Mencuccini, M.; Noije, T.V.; Borghetti, M. Assessing the effects of nitrogen deposition and climate on carbon isotope discrimination and intrinsic water-use efficiency of angiosperm and conifer trees under rising CO_2 conditions. *Glob. Chang. Biol.* **2012**, *18*, 2925–2944. [CrossRef] [PubMed]
17. Keenan, T.F.; Hollinger, D.Y.; Bohrer, G.; Dragoni, D.; Munger, J.W.; Schmid, H.P.; Richardson, A.D. Increase in forest water-use efficiency as atmospheric carbon dioxide concentrations rise. *Nature* **2013**, *499*, 324–327. [CrossRef] [PubMed]
18. Batista, K.D.; Araujo, W.L.; Antunes, W.C.; Cavatte, P.C.; Moraes, G.; Martins, S.C.V.; DaMatta, F.M. Photosynthetic limitations in coffee plants are chiefly governed by diffusive factors. *Trees-Struct. Funct.* **2012**, *26*, 459–468. [CrossRef]
19. Katul, G.G.; Palmroth, S.; Oren, R. Leaf stomatal responses to vapour pressure deficit under current and CO_2-enriched atmosphere explained by the economics of gas exchange. *Plant Cell Environ.* **2009**, *32*, 968–979. [CrossRef] [PubMed]
20. Zhou, S.; Yu, B.; Huang, Y.F.; Wang, G.Q. Daily underlying water use efficiency for Ameriflux sites. *J. Geophys. Res.-Biogeosci.* **2015**, *120*, 887–902. [CrossRef]
21. Zhao, M.S.; Heinsch, F.A.; Nemani, R.R.; Running, S.W. Improvements of the MODIS terrestrial gross and net primary production global data set. *Remote Sens. Environ.* **2005**, *95*, 164–176. [CrossRef]
22. Mu, Q.Z.; Zhao, M.S.; Heinsch, F.A.; Liu, M.L.; Tian, H.Q.; Running, S.W. Evaluating water stress controls on primary production in biogeochemical and remote sensing based models. *J. Geophys. Res. Biogeosci.* **2007**, *112*, 13. [CrossRef]
23. Su, Z. The surface energy balance system (SEBs) for estimation of turbulent heat fluxes. *Hydrol. Earth Syst. Sci.* **2002**, *6*, 85–99. [CrossRef]
24. Dolman, A.J.; Miralles, D.G.; de Jeu, R.A.M. Fifty years since Monteith's 1965 seminal paper: The emergence of global ecohydrology. *Ecohydrology* **2014**, *7*, 897–902. [CrossRef]
25. Lu, X.L.; Zhuang, Q.L. Evaluating evapotranspiration and water-use efficiency of terrestrial ecosystems in the conterminous united states using MODIS and Ameriflux data. *Remote Sens. Environ.* **2010**, *114*, 1924–1939. [CrossRef]
26. Meroni, M.; Rossini, M.; Guanter, L.; Alonso, L.; Rascher, U.; Colombo, R.; Moreno, J. Remote sensing of solar-induced chlorophyll fluorescence: Review of methods and applications. *Remote Sens. Environ.* **2009**, *113*, 2037–2051. [CrossRef]

27. Rossini, M.; Nedbal, L.; Guanter, L.; Ac, A.; Alonso, L.; Burkart, A.; Cogliati, S.; Colombo, R.; Damm, A.; Drusch, M.; et al. Red and far red sun-induced chlorophyll fluorescence as a measure of plant photosynthesis. *Geophys. Res. Lett.* **2015**, *42*, 1632–1639. [CrossRef]
28. Yang, X.; Tang, J.W.; Mustard, J.F.; Lee, J.E.; Rossini, M.; Joiner, J.; Munger, J.W.; Kornfeld, A.; Richardson, A.D. Solar-induced chlorophyll fluorescence that correlates with canopy photosynthesis on diurnal and seasonal scales in a temperate deciduous forest. *Geophys. Res. Lett.* **2015**, *42*, 2977–2987. [CrossRef]
29. Yang, H.L.; Yang, X.; Zhang, Y.G.; Heskel, M.A.; Lu, X.L.; Munger, J.W.; Sun, S.C.; Tang, J.W. Chlorophyll fluorescence tracks seasonal variations of photosynthesis from leaf to canopy in a temperate forest. *Glob. Chang. Biol.* **2017**, *23*, 2874–2886. [CrossRef] [PubMed]
30. Lee, J.E.; Frankenberg, C.; van der Tol, C.; Berry, J.A.; Guanter, L.; Boyce, C.K.; Fisher, J.B.; Morrow, E.; Worden, J.R.; Asefi, S.; et al. Forest productivity and water stress in Amazonia: Observations from GOSAT chlorophyll fluorescence. *Proc. R. Soc. B* **2013**, *280*. [CrossRef] [PubMed]
31. Yoshida, Y.; Joiner, J.; Tucker, C.; Berry, J.; Lee, J.E.; Walker, G.; Reichle, R.; Koster, R.; Lyapustin, A.; Wang, Y. The 2010 Russian drought impact on satellite measurements of solar-induced chlorophyll fluorescence: Insights from modeling and comparisons with parameters derived from satellite reflectances. *Remote Sens. Environ.* **2015**, *166*, 163–177. [CrossRef]
32. Lu, X.L.; Liu, Z.Q.; An, S.Q.; Miralles, D.G.; Maes, W.; Liu, Y.L.; Tang, J.W. Potential of solar-induced chlorophyll fluorescence to estimate transpiration in a temperate forest. *Agric. For. Meteorol.* **2018**, *252*, 75–87. [CrossRef]
33. Priestley, C.H.B.; Taylor, R.J. On the assessment of surface heat flux and evaporation using large scale parameters. *Mon. Weather Rev.* **1972**, *100*, 81–92. [CrossRef]
34. Zhao, F.; Guo, Y.Q.; Verhoef, W.; Gu, X.F.; Liu, L.Y.; Yang, G.J. A method to reconstruct the solar-induced canopy fluorescence spectrum from hyperspectral measurements. *Remote Sens.* **2014**, *6*, 10171–10192. [CrossRef]
35. Baldocchi, D.D. Assessing the eddy covariance technique for evaluating carbon dioxide exchange rates of ecosystems: Past, present and future. *Glob. Chang. Biol.* **2003**, *9*, 479–492. [CrossRef]
36. Jasechko, S.; Sharp, Z.D.; Gibson, J.J.; Birks, S.J.; Yi, Y.; Fawcett, P.J. Terrestrial water fluxes dominated by transpiration. *Nature* **2013**, *496*, 347–350. [CrossRef] [PubMed]
37. Cogliati, S.; Rossini, M.; Julitta, T.; Meroni, M.; Schickling, A.; Burkart, A.; Pinto, F.; Rascher, U.; Colombo, R. Continuous and long-term measurements of reflectance and sun-induced chlorophyll fluorescence by using novel automated field spectroscopy systems. *Remote Sens. Environ.* **2015**, *164*, 270–281. [CrossRef]
38. Rasmussen, C.E.; Williams, C.K.I. *Gaussian Processes for Machine Learning*; The MIT Press: Cambridge, MA, USA, 2006.
39. Verrelst, J.; van der Tol, C.; Magnani, F.; Sabater, N.; Rivera, J.P.; Mohammed, G.; Moreno, J. Evaluating the predictive power of sun-induced chlorophyll fluorescence to estimate net photosynthesis of vegetation canopies: A scope modeling study. *Remote Sens. Environ.* **2016**, *176*, 139–151. [CrossRef]
40. Liu, Z.Q.; Lu, X.L.; An, S.Q.; Heskel, M.; Yang, H.L.; Tang, J.W. Evaluating the advantage of multi-bands solar-induced chlorophyll fluorescence to derive canopy photosynthesis in a temperate forest. *Agric. For. Meteorol* **2018**. under review.
41. Zhang, Y.G.; Guanter, L.; Berry, J.A.; van der Tol, C.; Yang, X.; Tang, J.W.; Zhang, F.M. Model-based analysis of the relationship between sun-induced chlorophyll fluorescence and gross primary production for remote sensing applications. *Remote Sens. Environ.* **2016**, *187*, 145–155. [CrossRef]
42. Demmig-Adams, B.; Adams, W.W. Photosynthesis - harvesting sunlight safely. *Nature* **2000**, *403*, 371–374. [CrossRef] [PubMed]
43. Gu, L.H.; Fuentes, J.D.; Shugart, H.H.; Staebler, R.M.; Black, T.A. Responses of net ecosystem exchanges of carbon dioxide to changes in cloudiness: Results from two North American deciduous forests. *J. Geophys. Res. Atmos.* **1999**, *104*, 31421–31434. [CrossRef]
44. Guanter, L.; Alonso, L.; Gomez-Chova, L.; Amoros-Lopez, J.; Vila, J.; Moreno, J. Estimation of solar-induced vegetation fluorescence from space measurements. *Geophys. Res. Lett.* **2007**, *34*. [CrossRef]
45. Joiner, J.; Guanter, L.; Lindstrot, R.; Voigt, M.; Vasilkov, A.P.; Middleton, E.M.; Huemmrich, K.F.; Yoshida, Y.; Frankenberg, C. Global monitoring of terrestrial chlorophyll fluorescence from moderate-spectral-resolution near-infrared satellite measurements: Methodology, simulations, and application to GOME-2. *Atmos. Meas. Tech.* **2013**, *6*, 2803–2823. [CrossRef]

46. Joiner, J.; Yoshida, Y.; Vasilkov, A.P.; Middleton, E.M.; Campbell, P.K.E.; Yoshida, Y.; Kuze, A.; Corp, L.A. Filling-in of near-infrared solar lines by terrestrial fluorescence and other geophysical effects: Simulations and space-based observations from SCIAMACHY and GOSAT. *Atmos. Meas. Tech.* **2012**, *5*, 809–829. [CrossRef]
47. Frankenberg, C.; O'Dell, C.; Berry, J.; Guanter, L.; Joiner, J.; Kohler, P.; Pollock, R.; Taylor, T.E. Prospects for chlorophyll fluorescence remote sensing from the orbiting carbon observatory-2. *Remote Sens. Environ.* **2014**, *147*, 1–12. [CrossRef]
48. Papageorgiou, G.C. (Ed.) *Chlorophyll a Fluorescence: A Signature of Photosynthesis*; Advances in Photosynthesis and Respiration; Springer: Dordrecht, The Netherlands, 2004; Volume 19, pp. 1–42. ISBN 978-1-4020-3217-2.
49. Baker, N.R. Chlorophyll fluorescence: A probe of photosynthesis in vivo. *Annu. Rev. Plant Biol.* **2008**, *59*, 89–113. [CrossRef] [PubMed]
50. Frankenberg, C.; Fisher, J.B.; Worden, J.; Badgley, G.; Saatchi, S.S.; Lee, J.E.; Toon, G.C.; Butz, A.; Jung, M.; Kuze, A.; et al. New global observations of the terrestrial carbon cycle from GOSAT: Patterns of plant fluorescence with gross primary productivity. *Geophys. Res. Lett.* **2011**, *38*, L17706. [CrossRef]
51. Guanter, L.; Frankenberg, C.; Dudhia, A.; Lewis, P.E.; Gomez-Dans, J.; Kuze, A.; Suto, H.; Grainger, R.G. Retrieval and global assessment of terrestrial chlorophyll fluorescence from GOSAT space measurements. *Remote Sens. Environ.* **2012**, *121*, 236–251. [CrossRef]
52. Damm, A.; Guanter, L.; Paul-Limoges, E.; van der Tol, C.; Hueni, A.; Buchmann, N.; Eugster, W.; Ammann, C.; Schaepman, M.E. Far-red sun-induced chlorophyll fluorescence shows ecosystem-specific relationships to gross primary production: An assessment based on observational and modeling approaches. *Remote Sens. Environ.* **2015**, *166*, 91–105. [CrossRef]
53. Van der Tol, C.; Verhoef, W.; Timmermans, J.; Verhoef, A.; Su, Z. An integrated model of soil-canopy spectral radiances, photosynthesis, fluorescence, temperature and energy balance. *Biogeosciences* **2009**, *6*, 3109–3129. [CrossRef]
54. Kabela, E.D.; Hornbuckle, B.K.; Cosh, M.H.; Anderson, M.C.; Gleason, M.L. Dew frequency, duration, amount, and distribution in corn and soybean during SMEX05. *Agric. For. Meteorol.* **2009**, *149*, 11–24. [CrossRef]
55. Sakuratani, T. Studies on evapotranspiration from crops (2): Separate estimation of transpiration and evaporation from a soybean field without water shortage. *J. Agric. Meteorol.* **1987**, *42*, 309–317. [CrossRef]
56. Knyazikhin, Y.; Schull, M.A.; Stenberg, P.; Mottus, M.; Rautiainen, M.; Yang, Y.; Marshak, A.; Carmona, P.L.; Kaufmann, R.K.; Lewis, P.; et al. Hyperspectral remote sensing of foliar nitrogen content. *Proc. Natl. Acad. Sci. USA* **2013**, *110*, E185–E192. [CrossRef] [PubMed]
57. Liu, L.Y.; Liu, X.J.; Wang, Z.H.; Zhang, B. Measurement and analysis of bidirectional SIF emissions in wheat canopies. *IEEE Trans. Geosci. Remote Sens.* **2016**, *54*, 2640–2651. [CrossRef]
58. He, L.M.; Chen, J. M.; Liu, J.; Mo, G.; Joiner, J. Angular normalization of GOME-2 Sun-induced chlorophyll fluorescence observation as a better proxy of vegetation productivity. *Geophys. Res. Lett.* **2017**, *44*, 5691–5699. [CrossRef]
59. Köhler, P.; Guanter, L.; Kobayashi, H.; Sophia Walthershi, S.; Yang, W. Assessing the potential of sun-induced fluorescence and the canopy scattering coefficient to track large-scale vegetation dynamics in Amazon forests. *Remote Sens. Environ.* **2018**, *204*, 769–785. [CrossRef]